Development of Buffet Forcing Functions using Frequency-Dependent Coherence Factors

J. Micheal Ramey,* Martin K. Sekula,† David J. Piatak,‡ Patrick S. Heaney,§ and Francesco Soranna¶
NASA Langley Research Center, Hampton, VA, 23681

The current accepted approach to modeling launch vehicle transonic buffet environments is to acquire time-correlated unsteady pressure measurements at discrete locations on a model-scale wind-tunnel model and use these measurements to develop buffet forcing functions (BFFs). Part of the BFF development process is the application of coherence factors to account for the discrete nature of the pressure measurement used in the development of the BFFs. Presently, the Space Launch System (SLS) program divides the launch vehicle into distinct aerodynamic regions, within which, the coherence lengths are assumed to be constant. The coherence factors are computed by averaging the coherence function between sensors within the region over a specified frequency range. The present work validates and examines the impact of two proposed changes to the development of longitudinal coherence factors used in the development of launch vehicle BFFs. One change is to employ frequency-dependent coherence factors instead of coherence factors based on the mean of the coherence function. The second proposed change replaces the aerodynamic regions with a moving-segment approach that varies the calculated coherence lengths as a function of longitudinal location of the transducers. The impact of these approaches is examined using data from two rigid buffet model wind-tunnel tests: (1) a notional launch vehicle geometry through the comparison of discrete measurement-based BFFs to loads developed by continuous integration of unsteady pressure sensitive paint data and (2) the SLS Block 1 Cargo vehicle configuration for which BFFs have been previously developed using less-mature methods. The trends from this examination of updated coherence factor approaches ultimately result in more intuitive results than currently-accepted coherence methods.

Note to the Reader

The Space Launch System, including its predicted performance and certain other features and characteristics, have been defined by the U.S. government to be Sensitive But Unclassified (SBU). Information deemed to be SBU requires special protection and may not be disclosed to an international audience. To comply with SBU restrictions, details such as absolute values have been removed from some plots and figures in this paper.

I. Nomenclature

γ^2	=	magnitude-squared coherence
β	=	least-squares curve fit
L_c	=	coherence length
β_w	=	weighted least-squares curve fit
L_{eff}	=	effective coherence length
ζ_c	=	coherence factors
R^2	=	coefficient of determination
x_i	=	separation distance between transducers, x-direction
y_i	=	separation distance between transducers, y-direction

*Research Aerospace Engineer, Aeroelasticity Branch, MS 340, AIAA Member
†Senior Research Aerospace Engineer, Aeroelasticity Branch, MS 340
‡Assistant Branch Head, Aeroelasticity Branch, MS 340, AIAA Senior Member
§Research Aerospace Engineer, Aeroelasticity Branch, MS 340, AIAA Member
¶Research Aerospace Engineer, Aeroelasticity Branch, MS 340, AIAA Member

M	=	freestream Mach number
α	=	angle of attack
F	=	force
Φ^F	=	power spectral density of the force
$\Delta F_{\text{xyz,rms}}$	=	centerline buffet forcing functions in the x,y,z directions (mean removed), root-mean-square

II. Introduction

Launch vehicle transonic buffet environments involve the distribution of various levels of fluctuating pressures on the surface of the vehicle, some of which can be severe enough to generate large dynamic structural loads and vibratory responses. Transonic buffet occurs as a launch vehicle passes through the transonic regime, typically Mach numbers 0.8 to 1.2, where unsteady phenomena such as shock oscillations, boundary layer separation, turbulence and vortex shedding are prominent flow features. The unsteady aerodynamic forces produced by these phenomena can excite both global and local vehicle structural responses. The consequences of incorporating poorly characterized buffet environments into the design process can range from oversized structures that can reduce the vehicle capabilities to undersized structures that, in the worst case scenario, may result in structural failure [1–3]. It is thus imperative to appropriately characterize the transonic buffet environment.

Modeling buffet-related aerodynamic forces can be accomplished by developing buffet forcing functions (BFFs) – a series of orthogonal force time histories acting at various longitudinal stations on the vehicle centerline. Each orthogonal set of BFFs represents the net forces produced by the fluctuating surface pressures acting on a longitudinal segment of the vehicle. Buffet forcing functions are traditionally developed using experimentally-measured pressure time histories that are acquired using unsteady pressure transducers (PTs) embedded just below the surface of a rigid wind-tunnel model of a launch vehicle. Each of these discrete measurements is used to approximate the spatially-varying fluctuating surface pressures acting on a large wetted surface area of the vehicle. Accurate extrapolation of unsteady pressure variation across these large areas is not possible, thus the unsteady pressure is assumed to act in unison across a defined surface area. This simplification may result in an overprediction of the resultant loads. Therefore, coherence-based factors are employed to reduce the effective surface area used in the pressure integration, thereby approximating the effects of temporal and spatial variation in surface pressure [4].

To develop estimated buffet loads, NASA has conducted five rigid buffet model (RBM) tests on various configurations of the Space Launch System (SLS) launch vehicle and used the data to generate BFF databases for each configuration that was tested. The most mature database of BFFs for the Block 1 Crew configuration (Artemis I and II) was produced in 2014 based on data acquired on a 3-percent scale model tested at the Transonic Dynamics Tunnel (TDT) at the NASA Langley Research Center (LaRC), presented in Fig. 1a. During this test, a total of 472 PTs were axisymmetrically distributed at 37 longitudinal stations to produce a full-stack, time-correlated set of BFFs that are in use today. More detail about the test is available in Ref. [5].

The accuracy and validity of BFFs developed with coherence-based factors has long been a topic of research and discussion, but difficult to quantify. Recent advances in a measurement technique called unsteady pressure sensitive paint (uPSP) have provided a means to achieve this goal. In 2015, the Buffet Verification Test (BVT) was conducted at the NASA Ames Research Center (ARC) Unitary Plan Wind Tunnel (UPWT) 11-Foot Transonic Wind Tunnel (11-Ft TWT) [6]. During this test, a notional launch vehicle forebody (shown in Fig. 1b) was heavily instrumented with 213 PTs along with uPSP to improve the understanding of the transonic buffet environment, but also to substantiate the efficacy of uPSP. Subsequent comparisons of BFFs produced using discrete pressure measurements to BFFs produced by continuous surface integration of uPSP helped validate and identify shortcomings of currently-accepted BFF methodology and develop methods to improve them [7, 8].

One of the main conclusions from these comparisons is the need to employ frequency-dependent longitudinal coherence factors. Up to now, coherence factors were based on averaging the coherence function over a user-specified frequency range [9]. The spectral content of the resulting forcing functions will tend to be overpredicted at frequencies associated with low coherence and underpredicted at frequencies of high coherence. Replacing the single-value coherence factor that is based on an average coherence value with a vector of coherence factors at many frequencies should produce a more accurate representation of the BFF spectra.

The introduction of frequency-dependent coherence factors also necessitates a reexamination of how coherence factors are calculated and applied longitudinally on the vehicle. The current approach used to determine coherence factors requires the launch vehicle to be divided into longitudinal regions within which a single aerodynamic phenomenon is considered the dominant flow feature. The location of these boundaries are often selected based on engineering

(a) SLS Block 1 Crew model in the LaRC TDT.

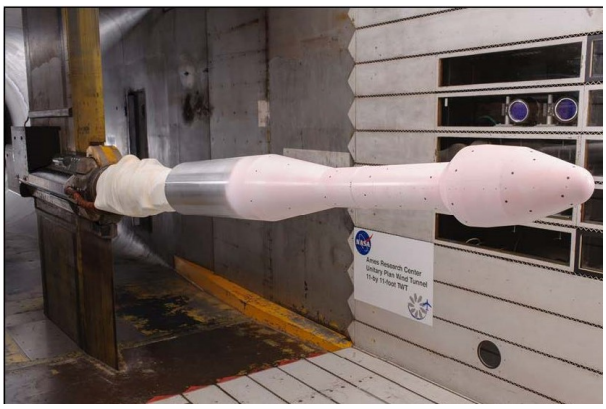

(b) Buffet Verification Test model in the ARC 11-Ft TWT.

Fig. 1 Rigid buffet wind-tunnel models.

judgment, guided by techniques such as shadowgraph and CFD. A recently developed tool to help guide aerodynamic region selection is an analysis technique that indicates where on the vehicle the station-to-station coherence does not fit the exponential decay function typical of turbulent flows. However, this analysis technique is based on mean coherence and assumes the longitudinal trends in coherence do not change as a function of frequency. This assumption may not always be the case, and thus aerodynamic regions should be defined for all frequency bins independently. Manually defining these aerodynamic regions for each frequency bin is impractical. Thus, an updated approach was developed that calculates coherence lengths that vary as a function of vehicle station without set aerodynamic regions.

This paper will provide an examination of the proposed modifications to the coherence factor analysis and its implementation in BFF development. An overview of how the coherence factors are calculated will be provided, including implementation with both mean coherence and frequency-dependent coherence factor approaches. This discussion will include an overview of how user-defined aerodynamic regions are selected and a detailed description of the proposed approach that eliminates the user-defined region approach will be provided. The validity and impact of these changes to the coherence factor analysis will be determined using uPSP data acquired during the Buffet Verification Test. Once validated, these BFF analysis improvements will be examined using wind-tunnel test data from the SLS Block 1 Crew vehicle. New BFFs will be compared to previously-developed BFFs for this SLS configuration that used the program-accepted coherence factor methods described in Section III.A.

III. Methodology

A. Program-Accepted BFF Development Methodology

Development of BFFs is aided by the Unified Buffet Methodology (UBM) analysis code, a MATLAB®-based analysis package in development at NASA LaRC. It is a flexible, spreadsheet-driven software that generates BFFs from experimentally-acquired pressure time histories following the general analysis outlined in Fig. 2. The underlying theory and implementation of the UBM code can be found in Ref. [4]. The present work focuses on the two steps of the analysis highlighted in the figure: calculation of the longitudinal coherence factors and aerodynamic region definition.

The calculation of longitudinal coherence factors in the current SLS program-accepted approach is a multistep process, the outline of which is as follows:

1) Aerodynamic regions of the vehicle (encompassing multiple transducer stations) are established based on major changes in the local aerodynamic environment that are often driven by vehicle geometry changes. This process employs a coefficient of determination analysis discussed in more detail later in this section.
2) The magnitude-squared coherence, γ^2, is calculated for all combinations of sectional BFFs (force-per-length) for all transducer stations within each aerodynamic region using the *mscohere* function in MATLAB®. A sample coherence function can be seen in Fig. 3a. See Ref. [4] for additional details on sectional BFFs.
3) An average value for each coherence function is calculated over a prescribed frequency range within the buffet bandwidth and plotted as a function of separation distance between transducers.

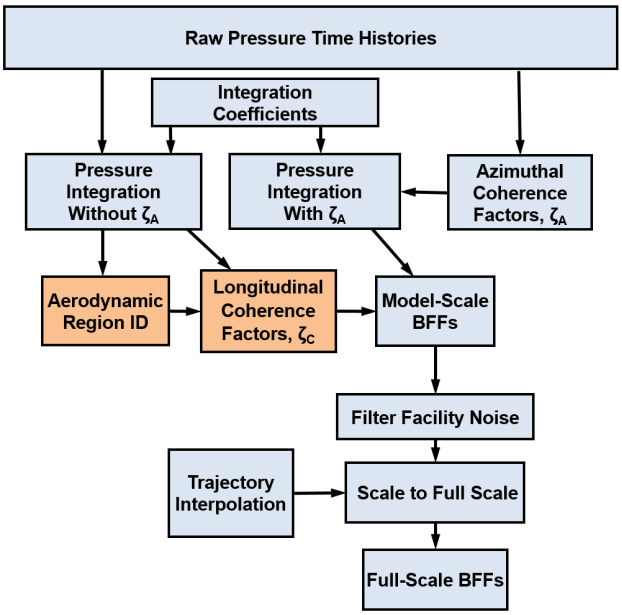

Fig. 2 Flowchart of BFF development process.

4) An exponential curve fit to the averaged coherence versus separation distance data points is determined using a weighted least-squares method. Using this curve fit, a coherence length, L_c, can be calculated by determining the separation distance at which the curve fit is equal to a user-defined nondimensional value. An example coherence versus transducer separation plot and curve fit can be seen in Fig. 3b.
5) The final step is to calculate the coherence factors, ζ_c. The coherence factor for each transducer station is a ratio of an effective length, L_{eff_i}, to the physical longitudinal length, $(L_z)_i$, of each integration segment of the vehicle.

$$(\zeta_c)_i = \frac{(L_{\text{eff}})_i}{(L_z)_i} \tag{1}$$

The effective length is defined as:

$$L_{\text{eff}_i} = \sqrt{(L_z)_i (L_c)_i} \tag{2}$$

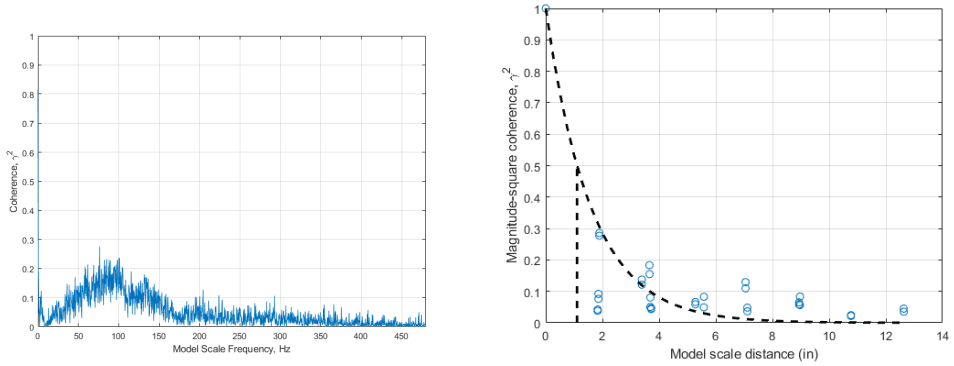

(a) Sample coherence function.

(b) Coherence length curve fit for sample aerodynamic region.

Fig. 3 Sample coherence calculations for the SLS Block 1 Crew model.

To provide rigor to the process of selecting aerodynamic regions, UBM includes an analysis to help identify transitions from one dominant aerodynamic phenomenon to another, suggested by drops in mean coherence. This

analysis employs a coefficient of determination, R^2, calculation to determine the quality of the curve fit with respect to the coherence data. This calculation uses pressure time histories for each vehicle azimuthal angle. R^2 calculations are typically conducted on a linear regression curve, but for the current analysis, the equation is modified for an exponential decay function:

$$R^2 = 1 - \frac{\sum_{i=1}^{N}(y_i - e^{\beta_w x_i})^2}{\sum_{i=1}^{N}(y_i - \overline{y})^2} \tag{3}$$

Where R^2 values are high, the analysis indicates the mean coherence is well approximated by the exponential decay function. Decreases in the R^2 values indicate that an exponential decay function does not model the coherence for that region well, and an increase afterwards indicates that a boundary has been crossed and a new aerodynamic region has begun. Using the local minimum as a guide, the user-defined boundaries should be placed after this local minimum. Example R^2 plots with associated user-defined regions selected can be seen in Fig. 5 for the BVT model and Fig. 14 for the SLS model.

Both the mean coherence analysis and the user-defined region analysis present drawbacks. Using the mean coherence across a broad frequency range overlooks the fact that different flow phenomena can have different correlation lengths at different frequencies. For example, a vortex shedding flow environment may have a relatively low frequency signature and can be associated with long coherence lengths. Meanwhile, shock-induced fluctuations downstream of protuberances are usually associated with very high frequency (in the aeroacoustic range), and typically have short coherence lengths. These nuances are smeared over using a mean coherence approach. Another drawback of mean coherence analysis is the spectral content of the resulting forcing functions will tend to be overpredicted at frequencies associated with low coherence and underpredicted at frequencies of high coherence. This mismatch is due to the nature of averaging itself: the lower frequency, long coherence length flow phenomena are integrated over a shorter length than physically appropriate, and higher frequency, short coherence length flow phenomena are integrated over a longer length than appropriate.

The main drawback of the user-defined region analysis is that the establishment of these regions still requires engineering judgment. It is often the case that while the pattern in R^2 values generally follows the OML changes, different azimuths sometimes produce different results. The R^2 calculations in these regions are influenced by localized environments and uneven transducer separation that produces a lack of clarity in boundary selection. Moving the established aerodynamic region boundary or even placing an additional boundary would both be acceptable interpretations of typical R^2 results. Furthermore, the region boundary might be established due to sharp OML changes rather than strict adherence to R^2 calculations. The next section will provide solutions to these drawbacks by introducing frequency-based coherence and the moving-segment aerodynamic region definition approaches to calculating coherence factors.

B. Updated BFF Methodology Approaches

The frequency-based coherence factor approach is an extension of the process for calculating mean coherence factors outlined in the previous section. Instead of averaging the coherence function over a user-specified frequency range, each frequency bin is treated as an independent quantity, each with its own exponential coherence decay function, resulting in a series of coherence factors that vary as a function of frequency. To apply these coherence factors to the BFF spectra, a Fast Fourier Transform (FFT) of each BFF is calculated to transfer the function into the frequency domain. A spline function is used to interpolate the coherence factors to each spectral line of the FFT, and the FFT coefficients are multiplied by the interpolated coherence factors. An inverse FFT is applied to these adjusted FFT coefficients to produce new BFFs in the time domain. For further details, see Ref. [8].

One of the significant challenges of implementing this frequency-dependent coherence factor analysis is the selection of longitudinal aerodynamic regions. Aerodynamic region definitions can vary as a function of frequency, as discussed above. Implementing the user-defined region approach to define these frequency-dependent boundaries is not practical since each frequency bin in the coherence analysis would need to be evaluated independently. Even a small window in the coherence calculation, such as $N = 2^8$, would require the entire boundary-determination process to be conducted 256 times, once for each frequency bin.

The time-intensive nature of the program-accepted R^2 approach used to determine aerodynamic regions, and ultimately the coherence factors, necessitated the need for an alternate approach to calculate coherence factors that did not require engineering judgment. This approach, called the moving-segment aerodynamic region approach (moving-segment approach for simplicity), eliminates the need to define aerodynamic boundaries by using a concept

employed by the R^2 analysis. A series of overlapping, longitudinal segments of the vehicle are defined, each with a set number of transducer stations. Moving longitudinally down the model, the coherence length for each overlapping segment is calculated using the same methods described in Section III.A. A minimum of three transducer stations are required in these segments to determine the exponential decay curve fit. Since the segments overlap, each station (other than first and last) is used to calculate multiple coherence lengths. To provide conservatism in this analysis, the largest value of these coherence lengths is chosen as the coherence length associated with the station being evaluated. A graphical description of this approach is presented in Fig. 4. Each of the coherence length calculations is represented by the red horizontal lines. In this example, the segment length is set to 3. The process is started with the first three stations, then the second through the fourth stations, and so on until the end of the vehicle is reached. The evaluation of the largest coherence length is represented by the green rectangle. Other than the first and last longitudinal station on the vehicle, each transducer station is used in the calculation of multiple coherence lengths. Unlike the user-defined region approach, where a single coherence length is assigned to an aerodynamic region of the vehicle, the resulting coherence lengths calculated by the moving-segment aerodynamic region approach can vary from station to station.

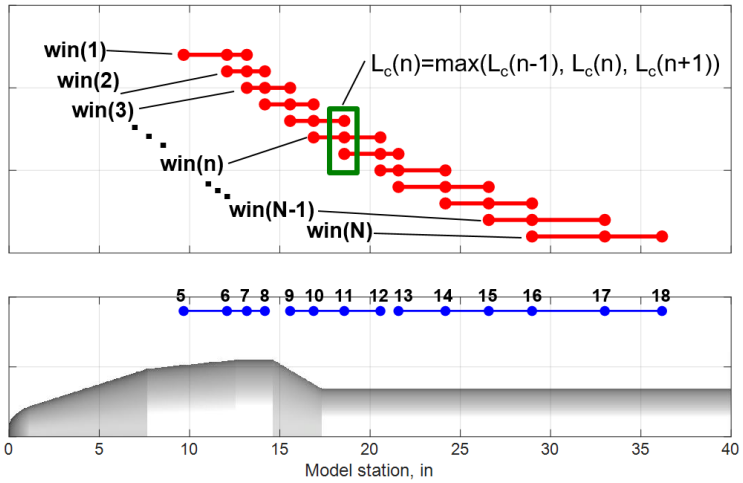

Fig. 4 Graphical representation of the moving-segment aerodynamic region approach.

IV. Results

In this section, the pressure data from two wind-tunnel test programs will be analyzed. In the first section, the accuracy of the updated approaches to developing BFFs is substantiated through the use of uPSP measurements taken during the BVT test. In the validation effort presented in Section IV.A, BFFs are developed using eight equally azimuthally-spaced discrete pressure measurements extracted from uPSP data, known as virtual transducers (VT). These BFFs are compared to BFFs developed by full integration of the continuous uPSP surface pressures for the same integration regions used for the discrete VT method. For brevity, this is referred to as the Full Integration (FI) method. In Section IV.B, comparisons between the updated approach and SLS program-accepted BFFs of the SLS Block 1 Crew RBM will be made, as uPSP measurements do not exist for the SLS model.

In order to better understand how the frequency-dependent coherence factors and the moving-segment analysis improves the fidelity of BFF development, four combinations of the BFF development approaches discussed above will be compared:

1) Mean coherence factors with user-defined aerodynamic regions (baseline, or MCU)
2) Mean coherence factors with moving-segment aerodynamic regions (MCM)
3) Frequency-dependent coherence factors with user-defined aerodynamic regions (FCU)
4) Frequency-dependent coherence factors with moving-segment aerodynamic regions (FCM)

A. Comparison of BFFs for coherence factor approaches for the BVT Test

BFFs developed using the four combinations of coherence analyses are compared to FI method BFFs, which are considered to be the most accurate representation of the time-varying forces acting on each segment of the model in

this paper. In this analysis, two test conditions are examined: $M = 0.92$ and $M = 1.10$, both at $\alpha = 0°$. The discrete measurement-based BFFs are developed using 8 axisymmetrically-spaced VTs at each transducer station. A previous study examined the sensitivity of the BFF fluctuation to the number of azimuthally-distributed discrete measurements used in the integration of pressures and the application of longitudinal coherence factors, Ref. [7]. This previous study only examined the mean coherence approach with user-defined regions, but it noted that the azimuthal sensor density has a direct impact on magnitude of the fluctuating forces. For an 8-sensor ring of transducers, a typical number of sensors per ring on a conventional rigid buffet model, the integration without azimuthal coherence adjustments produce on average an rms overprediction of 30 percent compared to the FI BFFs. This overprediction is also present in the current analysis.

1. Identification of aerodynamic regions

The user-defined regions are selected based on a coefficient of determination, R^2, analysis described in Section III.A. For the BVT model, the frequency range employed in calculating the mean coherence for this analysis was 0.5 to 800 Hz, model-scale. This analysis was performed for the two test conditions, using pressure measurements at eight azimuth angles around the model circumference and plotted in Fig. 5, which presents R^2 values versus station for $M = 0.92$ and $M = 1.10$ for $\alpha = 0°$. The analysis indicates that at $M = 0.92$ the flow field around this model geometry can be divided into three regions based on the drops in R^2 value. In this figure, vertical black lines were added to define the region boundaries. Based on shadowgraph observations (not presented), these three regions are dominated by attached flow on the hammerhead (labeled 1), separated flow on the frustum and directly downstream of the frustum (labeled 2), and reattached flow downstream of the separated flow region (labeled 3).

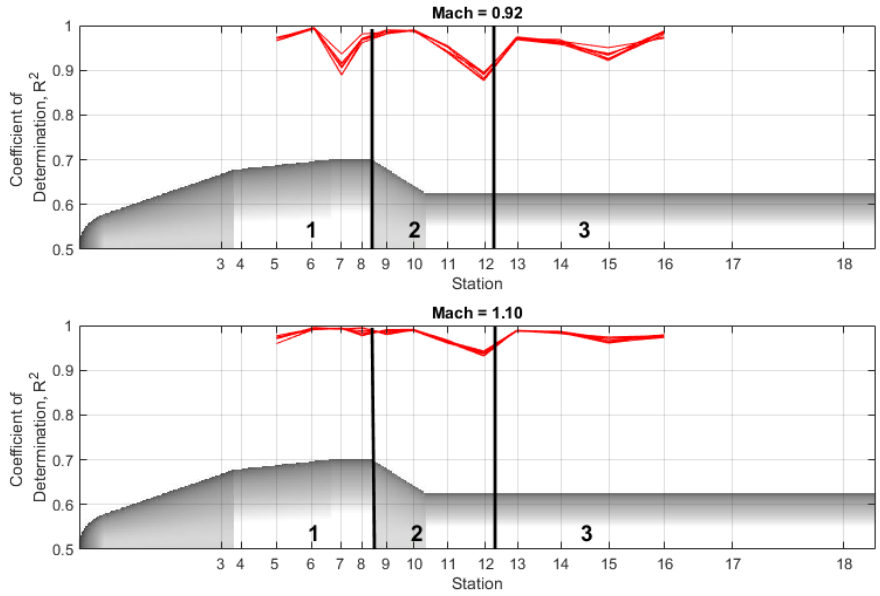

Fig. 5 Coefficient of determination for $M = 0.92$ and $M = 1.10, \alpha = 0°$.

Fig. 5 illustrates the engineering judgment involved in selecting these regions. The R^2 values increase sharply at $M = 0.92$ between transducers located between stations 7 and 8, but R^2 keeps increasing a little more for transducer station 9. This transducer ring is located on the frustum, downstream of a significant change in the model OML. Typically, the region boundary would be set between stations 7 and 8, but the sharp OML change at the starting point of the frustum is probably a more appropriate location for a boundary between aerodynamic regions. Although the R^2 values change somewhat for the $M = 1.10$ case, the differences did not warrant a change in the aerodynamic region definition compared to $M = 0.92$.

2. Discussion of mean coherence approach

The buffet forcing function root-mean-square with mean removed (i.e., standard deviation), $\Delta F_{\mathrm{xyz,rms}}$, values are presented in Fig. 6. Due to established conventions, these values will be referred to as rms. The BFFs were developed using coherence values based on 0.5 to 800 Hz frequency range. The MCU approach is represented by green unfilled squares and the MCM approach is represented by red unfilled diamonds. These VT-derived BFFs are compared to the FI-derived BFFs represented by blue solid circles. It should be noted that the FI-derived BFFs are not provided at the aft-most station, due to a lack of full-area coverage and increasing granularity of the uPSP measurements; VT measurements are unaffected and included to provide an additional station for the MCM approach.

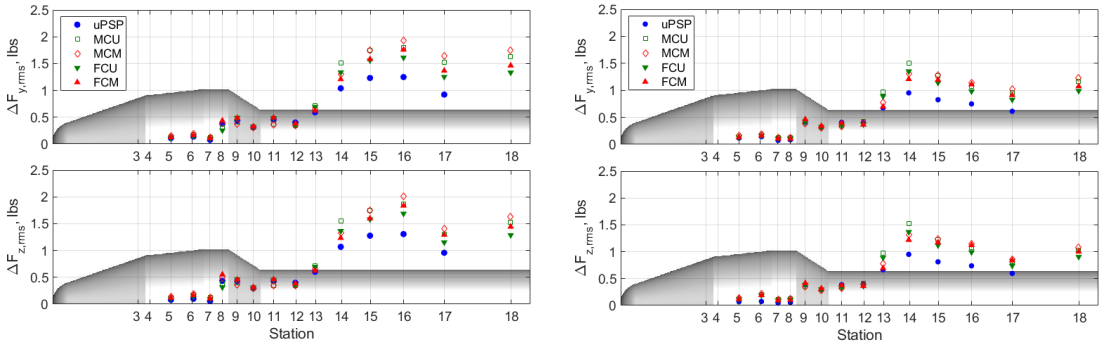

(a) $M = 0.92, \alpha = 0°$ **(b)** $M = 1.10, \alpha = 0°$

Fig. 6 Comparison of $\Delta F_{\mathrm{y,rms}}$ and $\Delta F_{\mathrm{z,rms}}$ trends for the four discrete VT methods and uPSP FI for $M = 0.92$ and $M = 1.10$.

The previous section described how the flow field around this model can be divided into three regions: an attached flow on the hammerhead, a separated flow on the frustum and directly downstream of the frustum, and a reattached flow downstream of the separated flow region. Since each of these regions has a unique flow field, comparisons of BFFs to FI-derived BFFs within each region are more appropriate and informative than general statements.

On the aft half of the hammerhead, where the flow is generally attached, the BFF rms levels are generally low. BFFs developed using both the MCU and MCM approaches are generally similar to, or slightly larger than, the rms levels from the FI BFFs. In the separated flow region, both approaches either slightly underpredict or are close to the rms levels of the FI BFFs. In the reattached flow region, the BFF rms levels are significantly higher than elsewhere on the model due to a combination of highly coherent flow and larger integration areas. The MCU and MCM approaches both overpredict the rms levels by up to 50 percent.

The source of the differences in BFF rms values between FI and the BFFs based on VT measurements can be better understood by examining the power spectral density functions (PSDs) of the various BFFs. PSDs of BFFs located at stations 9, 14, and 16 are presented in Fig. 7. The BFFs developed using the MCU approach are in red and MCM approach are in green, and are both compared to the FI-derived BFFs (blue).

In general, the VT BFFs significantly overpredict the high-frequency content relative to the FI-derived BFF PSDs, beyond that discussed in Ref. [7]. This trend is clear in all BFFs presented in Fig. 7. This overprediction occurs because the coherence factors employ the mean coherence approach that results in higher coherence factors due to low-frequency content in the flow that possess significantly higher coherence when compared to the high-frequency content. Another important observation is that in areas of the model where the coherence is high for low-frequencies, using the mean coherence approach to determine the coherence factors can result in underprediction of the BFFs at low frequencies. This issue occurs because using the mean coherence value results in an underestimation of high coherence values and an overestimation of low coherence values. This low-frequency underprediction is visible in the $M = 0.92$ case, Fig. 7a. For frequencies below 200 Hz, the BFF PSDs at station 9 are lower than the PSD for the integrated uPSP BFFs. The final observation is that the PSDs for the MCU and MCM approaches are identical in shape, except for a small amplitude offset. This offset is caused by differences in coherence factors, which are assumed constant across the entire frequency spectrum, and provides incentive to pursue the frequency-dependent coherence approach.

The coherence lengths for each transducer station for the MCU and MCM approaches are presented in Fig. 8a. The differences in the coherence factors, and the coherence lengths that the factors are derived from, arise from the

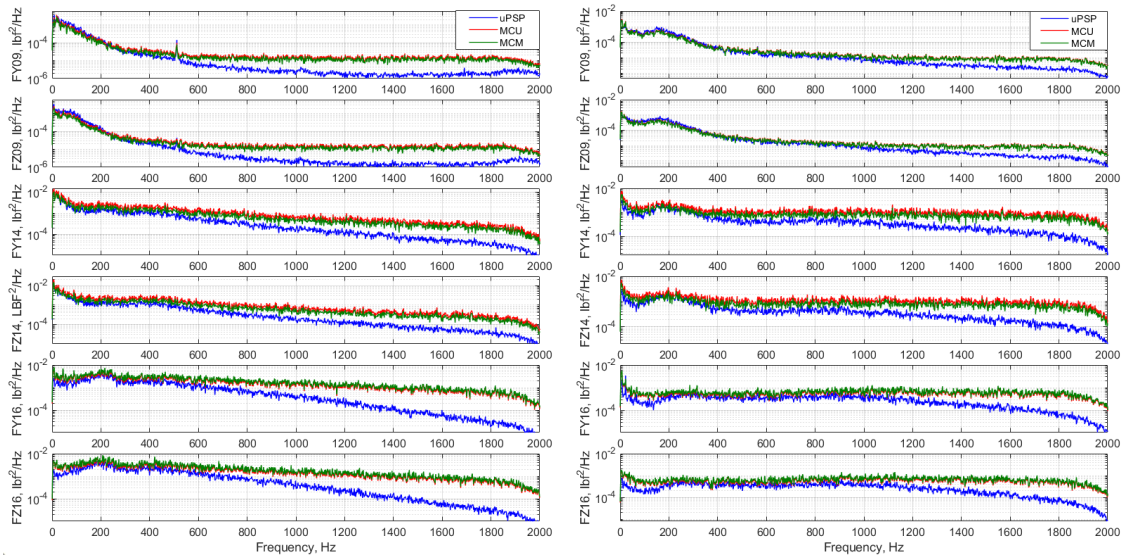

(a) $M = 0.92$**.** **(b)** $M = 1.10$**.**

Fig. 7 Effect of mean coherence factor approach on BFF PSDs in comparison to uPSP FI.

selection of transducer stations used in the coherence analysis. The green line represents the coherence lengths for each aerodynamic region identified by the MCU approach, or R^2 analysis (see Section III.A). Within each region the coherence length is constant. The red line represents the coherence lengths determined by the MCM approach. These MCM coherence lengths generally follow the user-defined region coherence lengths, except in the area near the transition from separated flow to reattached flow, approximately station 12 to station 16 (see Fig. 8a). At the forward end of this longitudinal range, the MCM approach predicts a lower coherence length than the MCU approach. Moving further aft, the MCM coherence length increases and eventually reaches a value larger than the user-defined region coherence length. It should be noted that for the reattached flow region (region 3 in Fig. 5), the value of user-defined region coherence length falls in between the maximum and minimum MCM coherence lengths, although it is not an average value of the MCM coherence lengths.

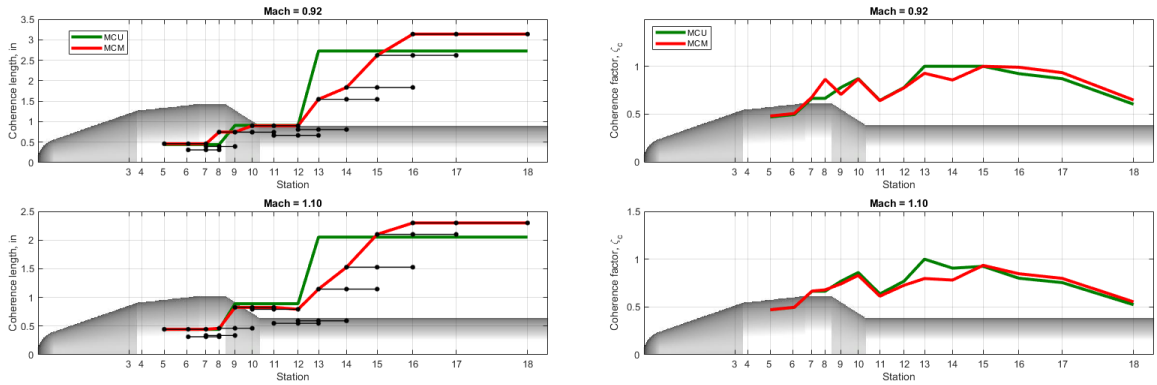

(a) Coherence Lengths. **(b) Coherence Factors.**

Fig. 8 Coherence lengths and factors based on MCU and MCM approaches.

The black lines in Fig. 8a span three adjacent transducer stations and indicate the coherence lengths for each three-station region that the MCM coherence length (red line) is based on. These lines demonstrate that the change in coherence lengths between different aerodynamic phenomena can be somewhat gradual in areas where a change

in vehicle OML does not exist, such as between the separated and reattached flow regions. These are spread over a significant portion of the model, and are not the hard boundaries between aerodynamic regions assumed by the MCU. This gradual change can reduce the coherence factors in such a region, as presented in Fig. 8b.

3. Discussion of frequency-dependent coherence approach

The previous section identified some shortcomings in using the mean coherence approach to develop coherence factors. These shortcomings included overprediction of high-frequency BFF content and underprediction of some BFFs at low frequencies. These issues can be attributed in part to the fact that coherence varies with frequency. Based on these observations, a frequency-dependent coherence factor approach has been implemented in developing BFFs.

The rms values for BFFs adjusted using frequency-dependent coherence factors are presented in Fig. 6. The BFFs developed using the FCU approach are represented by solid green triangles, while BFFs developed using the FCM approach, discussed in Section III.B, are represented by solid red triangles. These VT-derived BFFs are compared to the FI-derived BFFs represented by blue solid circles. In general, forward of station 13, which encompasses the attached flow region on the hammerhead and the separated flow region, the combination of frequency-dependent coherence factors with either of the two aerodynamic region definition approaches yields BFF rms trends that track the uPSP fluctuation levels. The only exception to this observation occurs at $M = 0.92$, station 8. At this condition and location, the FCU approach underpredicted the level of fluctuation. This underprediction may be associated with the engineering judgment used in selecting aerodynamic regions also discussed in Section III.B. In the reattached flow region (region 3), and in the transition region at the beginning of it, the FCU and FCM approaches overpredict the BFF fluctuation levels (i.e. rms), but less so than the BFFs adjusted with mean coherence factors. For the FCU and FCM approaches, the overall trends in BFF fluctuation levels follow those noted for the mean-coherence factors. In the transition region between separated and reattached flow, the FCM approach followed the FI-derived BFFs more closely, while further downstream, the FCU approach resulted in overall fluctuation levels closer to the FI uPSP fluctuation levels.

The improved estimate of BFF spectral content using the FCU and FCM approaches is illustrated in the PSDs presented in Fig. 9. The PSDs presented in this figure correspond to those presented in Fig. 7, except frequency-dependent coherence factors are applied instead of mean coherence factors. A comparison of Figs. 7 and 9 indicates that the frequency-dependent coherence factors result in BFFs that more closely match within the low-frequency range of the PSDs and a lesser – overprediction of the high frequency component of the PSDs.

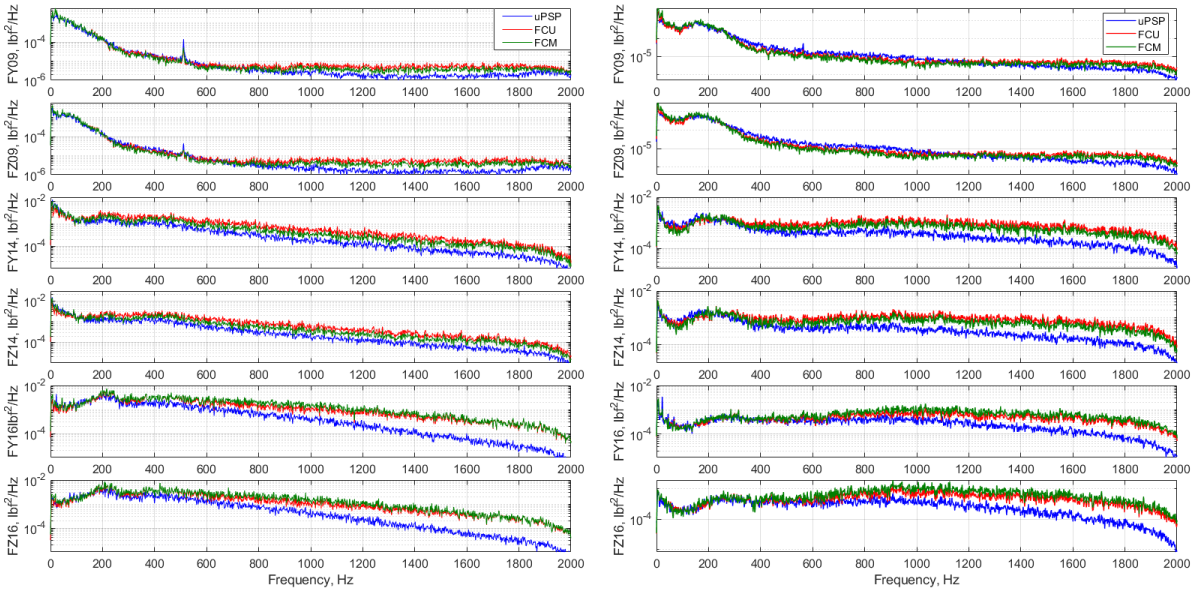

(a) $M = 0.92$**.** **(b)** $M = 1.10$**.**

Fig. 9 Effect of frequency-dependent coherence factor approach on BFF PSDs in comparison to uPSP FI.

The frequency-dependent coherence factors employed in developing these BFFs are based on coherence lengths that are a function of frequency and longitudinal station. These are presented as contour plots in Figs. 10 and 11 for

$M = 0.92$ and $M = 1.10$ test conditions, respectively. Both the FCU and FCM approaches are presented for each condition. The aerodynamic region boundaries are clearly discernible in the user-defined region approaches, Figs. 10a and 11a. The coherence lengths change at approximately stations 9 and 13 as defined by the boundaries in Fig. 5. The coherence lengths based on the moving-segment approaches change less abruptly, and continuously vary both as a function of frequency and longitudinal station. These two sets of plots indicate that in the separated flow region, the largest coherence lengths occur at low frequencies (below 200 Hz), while in the reattached flow region the coherence lengths increase as a function of frequency and reach a maximum at a frequency of approximately 500 Hz and 1000 Hz (for $M = 0.92$ and 1.10, respectively) before reducing again. The moving-segment approaches also indicates that the coherence lengths in the reattached flow region are higher further downstream from the frustum. These results suggest that the moving-segment approach to aerodynamic region definition provides a higher fidelity and more spatially accurate estimate of coherence length.

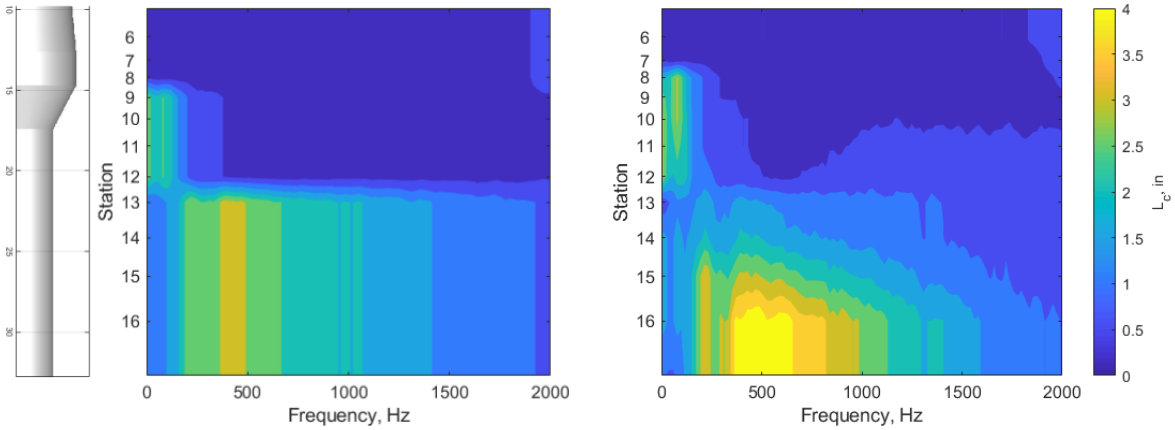

(a) User-defined aerodynamic regions. **(b) Moving-segment aerodynamic regions.**

Fig. 10 Frequency-dependent coherence lengths, inches, $M = 0.92$.

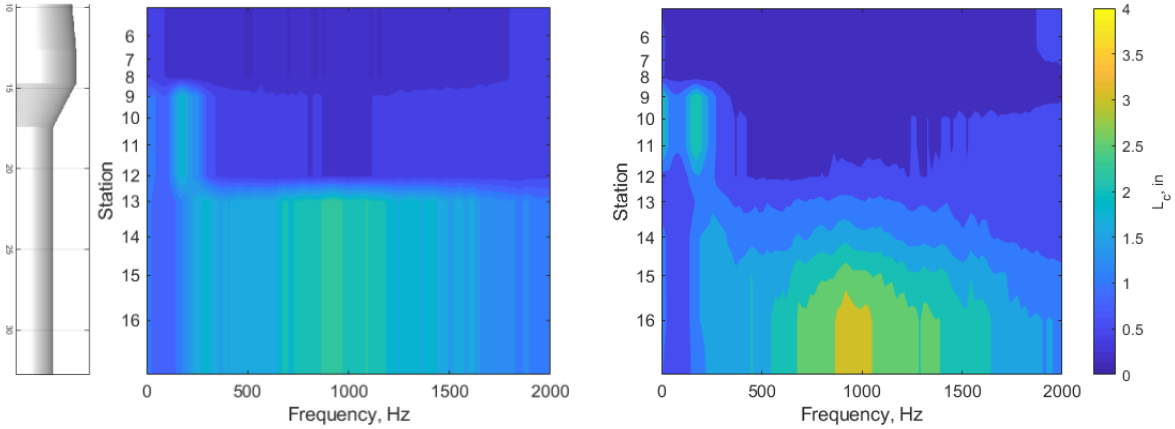

(a) User-defined aerodynamic regions. **(b) Moving-segment aerodynamic approach.**

Fig. 11 Frequency-dependent coherence lengths, inches, $M = 1.10$.

These coherence lengths are combined with the longitudinal length of each vehicle segment to determine the frequency-dependent coherence factors, presented in Figs. 12 and 13. The reattached flow region coherence factors display the advantage of the moving-segment approach over the user-defined set of aerodynamic regions. The user-defined coherence lengths are artificially increased by the selected location of the aerodynamic boundary between the separated

flow and reattached flow regions. This leads to higher coherence factors in this transition region compared to the moving-segment analysis.

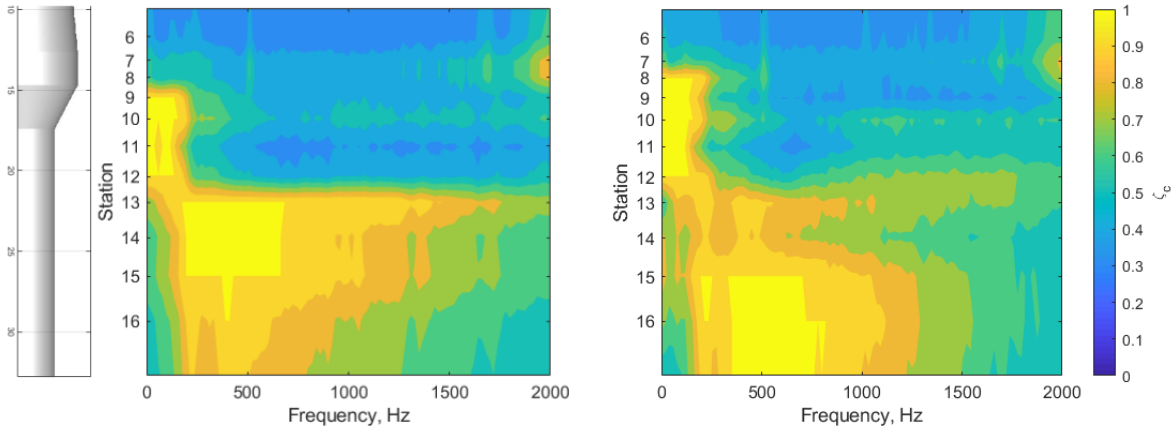

(a) User-defined aerodynamic regions. **(b) Moving-segment aerodynamic regions.**

Fig. 12 Frequency-dependent coherence factors, $M = 0.92$.

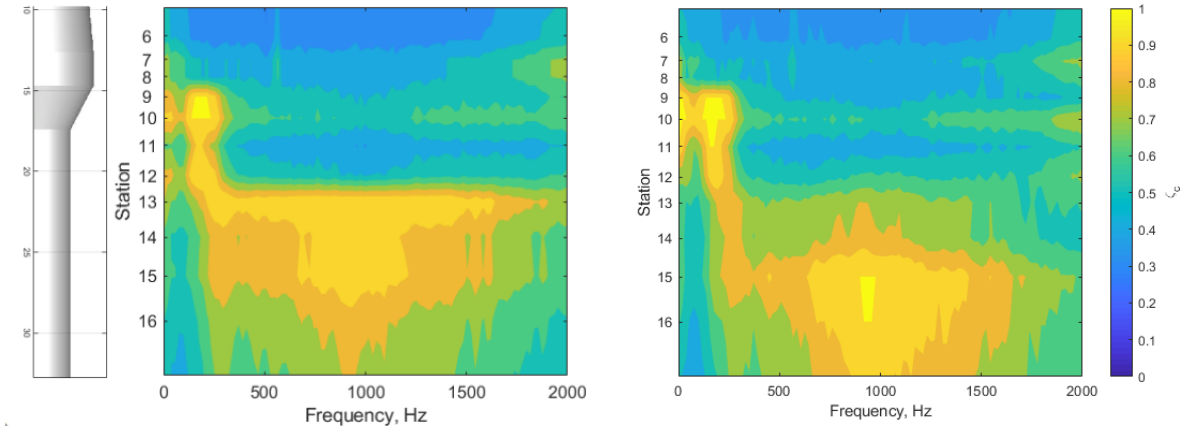

(a) User-defined aerodynamic regions. **(b) Moving-segment aerodynamic regions.**

Fig. 13 Frequency-dependent coherence factors, $M = 1.10$.

B. Comparison of BFF Improvement Methods for the SLS Block 1 Crew

The results from the BVT test data analysis provided a comparison of BFFs developed using the four different coherence factor calculation approaches and compared them to BFFs developed using the uPSP-based FI integration. Using the FI data as the most ideal estimate of the BVT BFFs, the results suggest that the FCM approach results in the most accurate estimate of discrete measurement BFFs. While informative, the BVT model is based on a notional geometry selected for its predisposition to produce a significant buffet environment to aid in the study of transonic buffet phenomena. To provide a more realistic test case, the impact of frequency-dependent and moving-segment coherence approaches will be examined in this section on the SLS Block 1 Crew launch vehicle.

Two key differences between the BVT test measurements and SLS test measurements should be emphasized. First, the SLS test employed discrete pressure transducer measurements, while the BVT analyses employed VT measurements that were simulated by extracting uPSP data for a small area at a simulated transducer location. The SLS Block 1 Crew wind-tunnel test did not include uPSP measurements, and therefore, the original BFFs developed with the proposed

techniques will be compared against the BFFs developed for the SLS program (referred to as baseline). The baseline BFFs, developed using mean coherence factors and user-defined aerodynamic regions, will be compared against the other three combinations of coherence analysis approaches enumerated at the beginning of the results section.

Throughout the SLS vehicle comparisons, all frequency-dependent coherence factors use a window size of 512 samples and the moving-segment analysis uses a 3-transducer station-spanning segment length. To match the baseline database, azimuthal coherence factors are applied to the first 19 stations of the vehicle and wind tunnel-generated tones are also attenuated for all BFFs using an SVD/PCA approach described in Ref. [4]. In the present analysis, the full-scale BFFs analysis is limited to buffet-related spectral content at two test conditions: $M = 0.90$ and 1.10, both at $\alpha = 0°$.

1. Identification of aerodynamic regions

The user-defined regions for the SLS test were selected based on the R^2 analysis described in Section III.A. This analysis was performed for both test conditions using the pressure measurements at eight azimuth angles (0 through 315 degrees, in 45 degree increments) around the model circumference of the core and plotted in Fig. 14. The R^2 analysis indicates that the SLS core can be divided into 7 aerodynamic regions (as opposed to 3 for the BVT model). These include (labeled 1 through 7 in the figure, respectively):

1) Forward section of the launch-abort system (LAS)
2) Downstream of the LAS nozzles to the crew vehicle ogive fairing
3) Aft section of the crew vehicle to the end of the service module
4) Service module to the end of the stage adapter
5) Forward half of the core stage to the SRB forward attachment hardware
6) Aft of the SRB forward attachment hardware to approximately three-quarters of the length of the SRB
7) Aftmost segment of the core

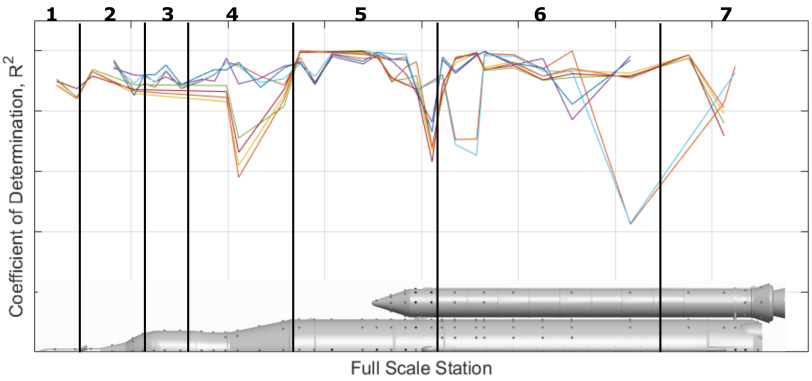

(a) $M = 0.90, \alpha = 0°$**.**

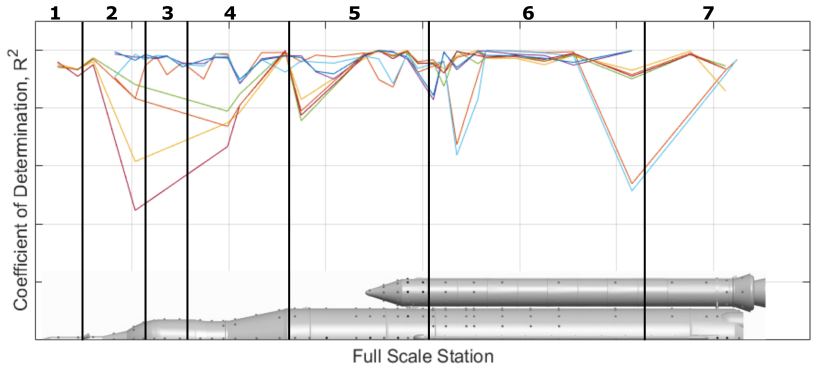

(b) $M = 1.10, \alpha = 0°$**.**

Fig. 14 Coefficient of determination for the SLS core.

The figures illustrate the difficulties with selecting the aerodynamic boundaries for this more complex OML. The R^2 functions can vary significantly from azimuth to azimuth. These differences can be caused by sensor spacing and local differences in the aerodynamic environment caused by protuberances and other azimuthal variations in the OML as well as model attitude relative to the free stream. When trends in the R^2 values do not provide a clear indication of boundary placement, engineering judgment and experience are needed to select boundary locations.

2. Impact of coherence factor approaches on $\Delta F_{y,rms}$ and $\Delta F_{z,rms}$

The improved comparison relative to FI-derived BFFs of the frequency dependent coherence factors and moving segment analysis was established in section IV.A.2 for a simple, axisymmetric vehicle geometry. This section examines how using mean coherence factors versus frequency-dependent coherence factors and user defined aerodynamic regions versus moving-segment analysis affect BFFs developed for a multibody launch vehicle, the SLS Block 1 Crew vehicle.

Figures 15 and 16 present the SLS Core BFF rms values ($\Delta F_{y,rms}$ and $\Delta F_{z,rms}$) for the four combinations of coherence factor analysis approaches: the baseline (MCU) approach represented by green unfilled squares; the MCM approach represented by red unfilled diamonds; the FCU approach represented by green solid triangles; and the FCM approach, represented by red solid triangles.

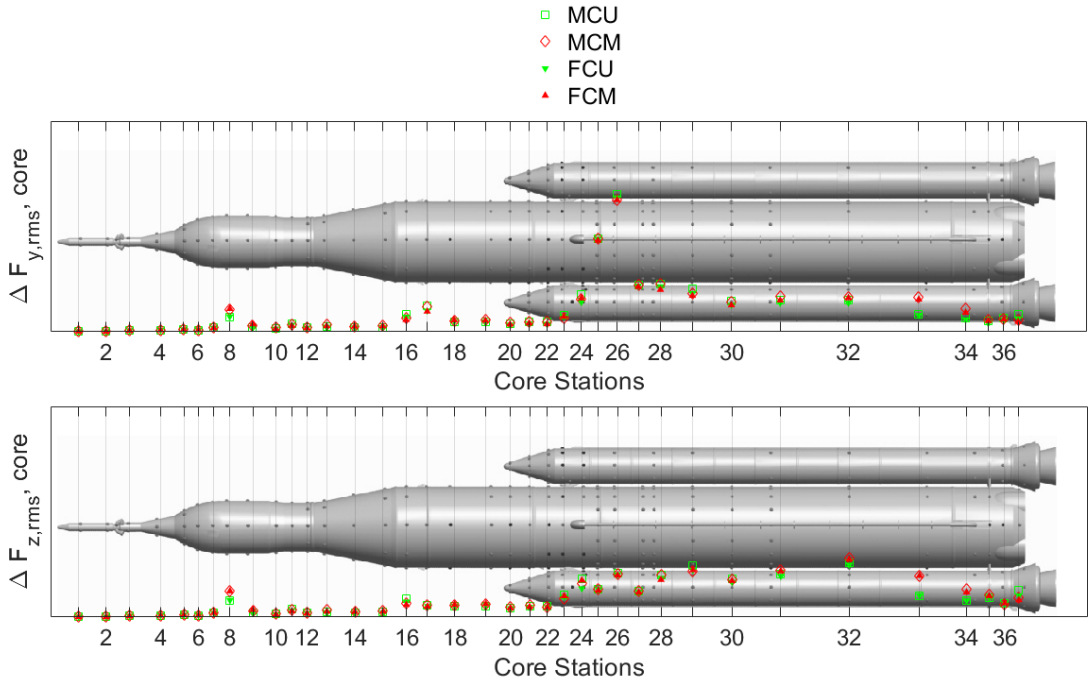

Fig. 15 Longitudinal distribution of BFFs for the core of the SLS Block 1 Crew vehicle, $M = 0.90, \alpha = 0°$.

Two trends in the BFF rms values are identifiable in Figs. 15 and 16. Forward of the SRB forward attachment, the rms levels for the BFFs developed using the four coherence factor approaches generally matched well. In the areas of the vehicles where the rms levels differed (stations 8, 16, 17, and aft of the SRB forward attachment), the choice of using the moving-segment analysis or the user-defined regions had a larger influence on the differences in rms levels than whether frequency-dependent or mean coherence factors are employed.

For the $M = 0.90$ case, the MCM- and FCM-derived BFFs for station 8, the location of a terminal shock, overpredict the rms by 30 percent compared to the baseline (MCU approach) and FCU approach. At stations 16 and 17, downstream of the expansion corner aft of the stage adapter, the MCM and FCM approaches underpredict the BFF rms values by 25 percent, relative to baseline and FCU approaches. In the vicinity of the SRB forward attachment hardware, stations 24-30, the FCM and MCM approaches resulted in lower rms values than the baseline and FCU approaches. Further aft, stations 32 through 34, the FCM and MCM approaches result in higher BFF rms levels.

The $M = 1.10$ case generally follows the same trends described for $M = 0.90$, but the differences in rms levels

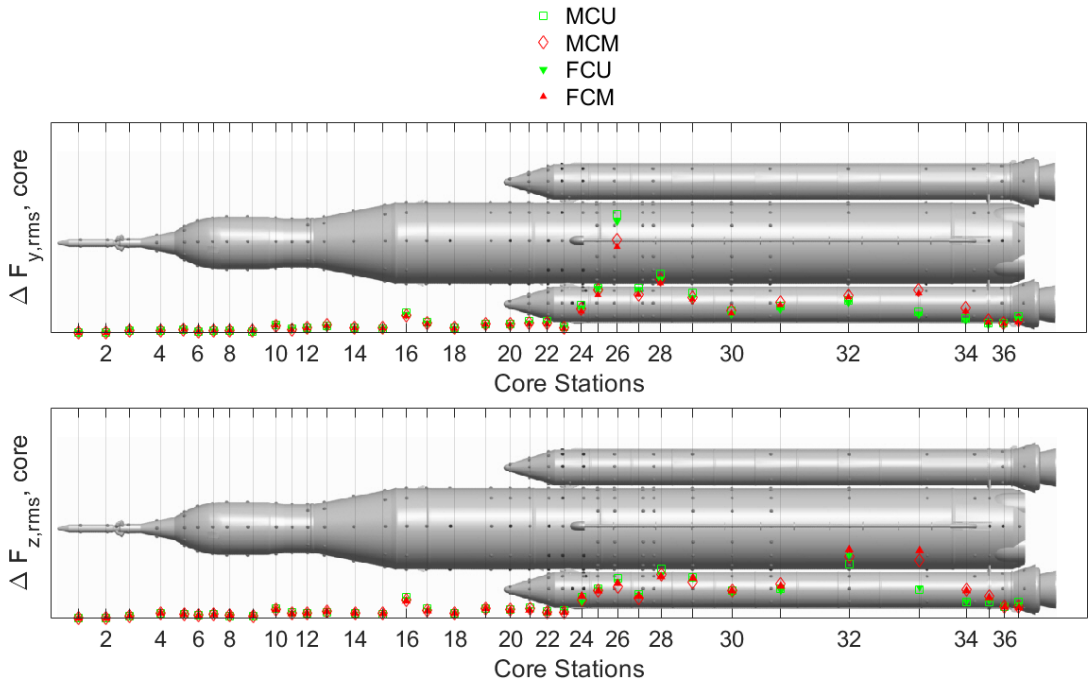

Fig. 16 Longitudinal distribution of BFFs for the core of the SLS Block 1 Crew vehicle, $M = 1.10, \alpha = 0°$**.**

between BFFs based on coherence factors developed using the moving-segment and user-defined approaches is much more pronounced.

3. Impact of Coherence Factor Approach on Coherence Lengths

In the previous section, trends in BFF rms values indicated that the choice of coherence factor development approach can, for some conditions, significantly affect the resulting BFFs. Figures 17 and 18 provide the coherence lengths and factors based on the two mean coherence approaches, MCU (baseline) and MCM. The green lines represent the MCU approach and the red lines represent the MCM approach. The aerodynamic boundaries are clearly discernable in the user-defined coherence lengths plot, since the coherence lengths are assumed constant across each defined aerodynamic region. Changes in coherence lengths for the MCM approach generally follow the MCU approach, but include some differences. In the transition area between aerodynamic regions, the MCM approach results in lower coherence lengths, but in the aft section of each aerodynamic region, the MCM approach predicts longer coherence lengths for the $M = 0.90$ case, while similar coherence lengths for the $M = 1.10$ case. The transition from aerodynamic region 5 to 6 (station 24/25) is more gradual for the MCM approach, resulting in lower coherence lengths for transducer stations 24 through 30 – the region of the vehicle with the largest BFF rms values (See Figures 17 and 18). Even though there is a large change in coherence length for these stations, the coherence factors show a minimal decrease. This observation indicates that the coherence lengths are of comparable value to the longitudinal integration lengths associated with each ring of sensors, and thereby having a minimal effect on the BFF rms levels for these stations.

At $M = 0.90$, the much longer coherence lengths in the vicinity of station 8 developed using the MCM approach resulted in the higher rms values at that station. The constant value of the MCM across stations 8-10 implies that a possibly more appropriate choice for the user-defined aerodynamic region 3 could have been slightly further back on the vehicle. For stations 16 and 17, the coherence length and subsequently the rms levels are lower. This decrease in coherence lengths relative to the MCU approach is consistent with the other regions of the vehicle where a transition between aerodynamic regions occurs. The MCM approach indicates a more gradual (longitudinally spread out) change in the coherence of the local flow field compared to the abrupt change assumed by the MCU approach. These observations also apply to the $M = 1.10$ case.

Figures 19 and 20 present the FCU and FCM approaches for $M = 0.90$ and $M = 1.10$, respectively. These contour

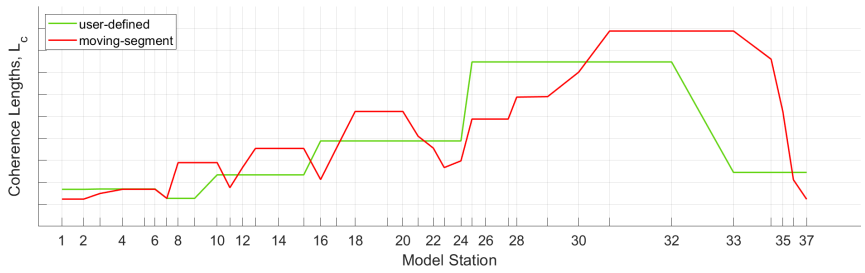

(a) Coherence Lengths.

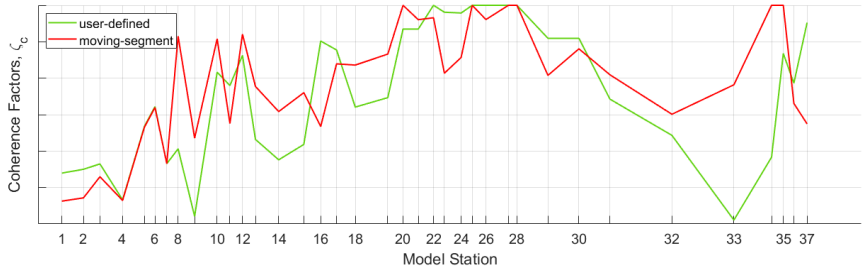

(b) Coherence Factors.

Fig. 17 Longitudinal distribution of coherence factors for the core of the SLS Block 1 Crew vehicle at $M = 0.90, \alpha = 0°$.

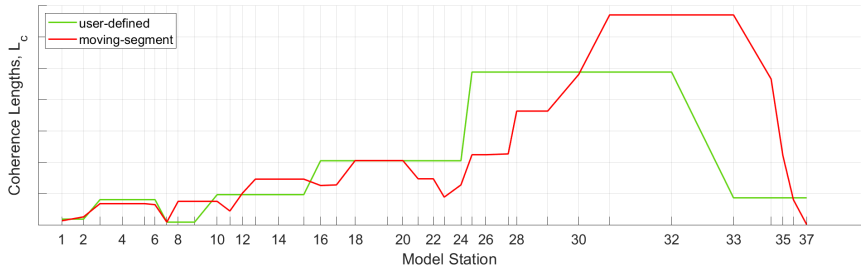

(a) Coherence Lengths.

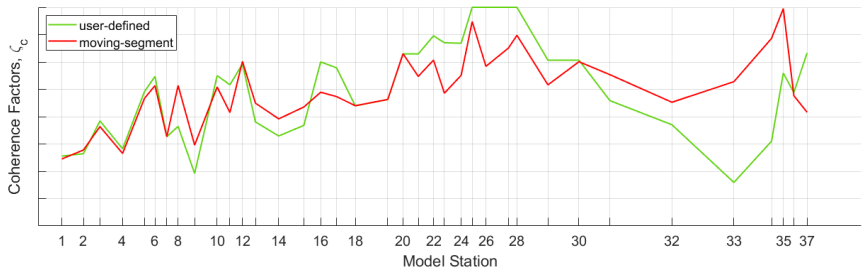

(b) Coherence Factors.

Fig. 18 Longitudinal distribution of coherence factors for the core of the SLS Block 1 Crew vehicle at $M = 1.10, \alpha = 0°$.

plots present coherence factors as a function of vehicle station and frequency. The color intensity represents the coherence factor, while the abscissa represents the frequency and the vehicle station is presented on the ordinate. The aerodynamic regions for the user-defined cases correspond to the regions identified in Fig. 14. At low frequencies, the FCU approach results in coherence factors that abruptly increase for a range of low frequencies when a user-defined

aerodynamic boundary is crossed. The FCM approach generally results in higher low-frequency coherence factors across longer regions of the vehicle. In the vicinity of the SRB forward attachment hardware, the FCM approach results in large coherence factors limited to much narrower bands of frequencies than the FCU approach. These bands are harmonics of the fundamental shedding frequency involving a coupling vortex shedding from the SRB forward attachment hardware and shocks that form on either side of the SRBs [10–12]. Further down the vehicle, the first harmonic of this phenomenon, while distinct in both the FCU and FCM approaches, results in higher coherence factors using the FCM approach. These observations also hold true for the $M = 1.10$ case.

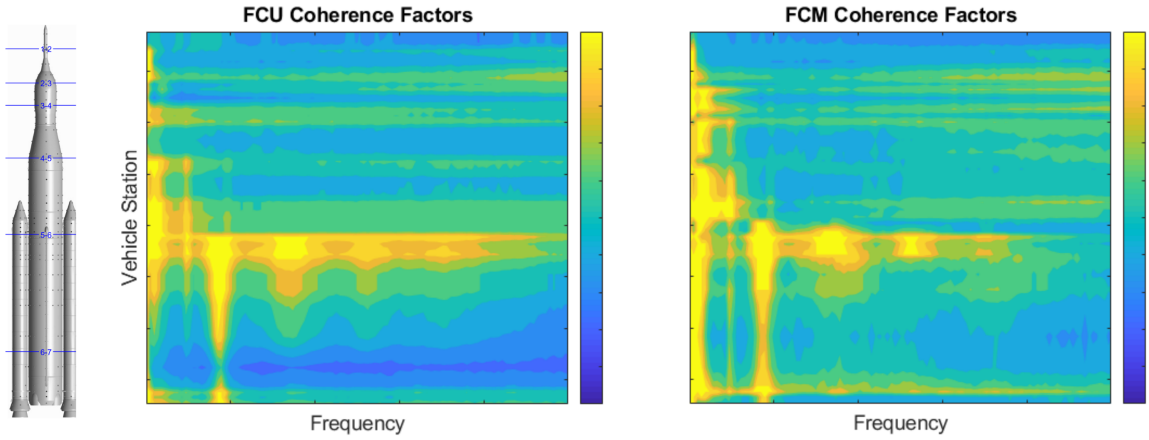

Fig. 19 Coherence factors, ζ_c, comparison for $M = 0.90, \alpha = 0°$.

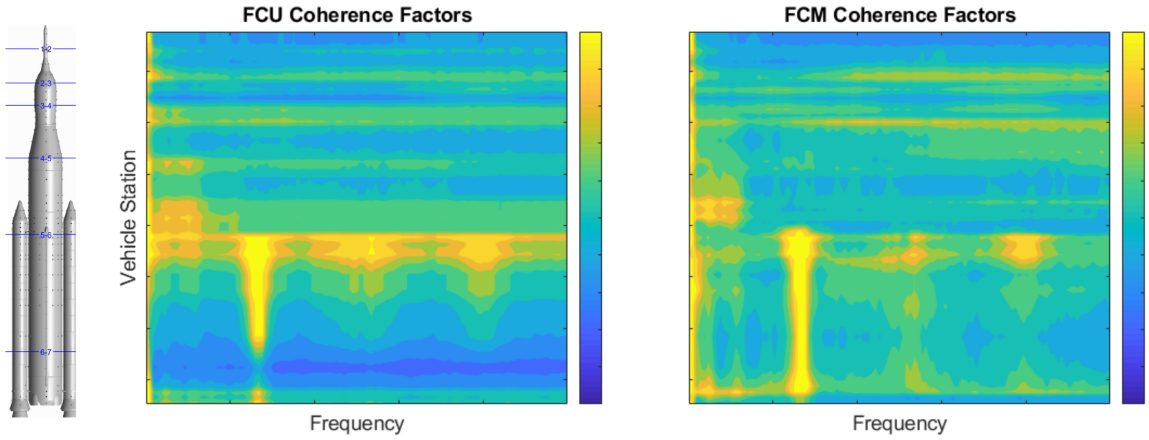

Fig. 20 Coherence factors, ζ_c, comparison for $M = 1.10, \alpha = 0°$.

4. Power Spectral Density Functions

To more fully understand the impact of the various coherence factor approaches have on the resulting BFFs, the spectral content of BFFs is examined at four stations where the coherence factors significantly change the BFF rms values in Figs. 15 and 16. These stations are: station 8, downstream of the crew vehicle; station 16, downstream of the stage adapter shoulder; station 26, downstream of the forward attachment (and highest BFF loads on the vehicle); and station 33, in the multibody region near the aft end of the model. The PSDs of the lateral (y) and vertical (z) direction BFFs at these stations for both $M = 0.90$ and $M = 1.10$ are presented in Fig. 21. The baseline (or MCU) approach is presented in blue; the MCM approach is presented in red; the FCU approach is presented in green; and the FCM approach is presented in black.

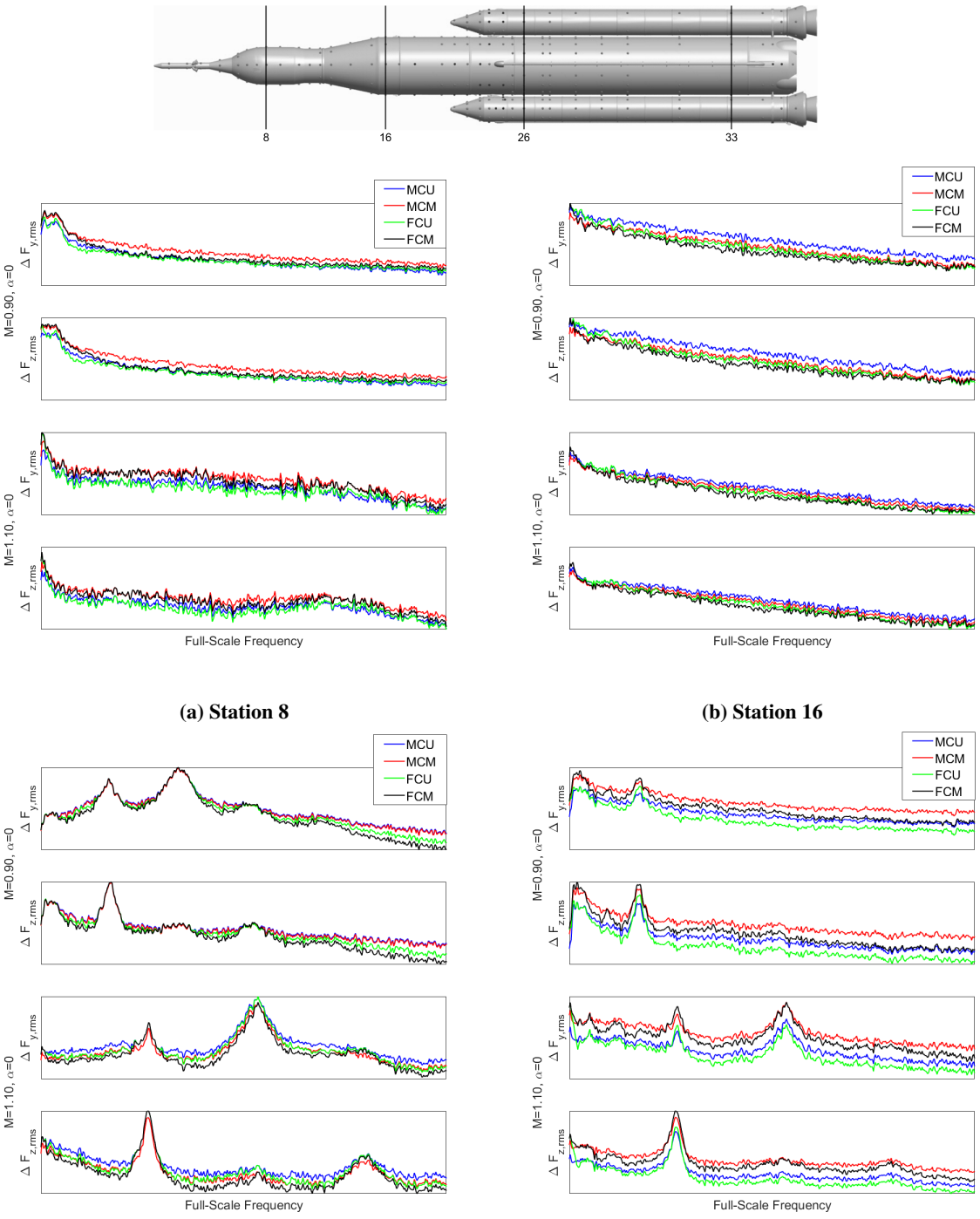

(a) Station 8 **(b) Station 16**

(c) Station 26 **(d) Station 33**

Fig. 21 Power spectral densities, Φ^F, of y- and z-direction BFFs of selected stations.

The BFFs at these four stations represent different aerodynamic environments, and therefore, the method to calculate the coherence factors may have a unique effect on the resulting BFFs, but there are also some general similarities notable in the PSDs. The spectra of the BFFs developed using the four coherence factor approaches exhibit the same overall shape – the peaks do not shift in frequency, nor do they become broader. BFFs developed using mean coherence

factors, MCU and MCM approaches, change the amplitude of the entire PSD by the same amount resulting in an upward or downward shift of the PSDs. BFFs developed using the frequency-dependent coherence factors, FCU and FCM approaches, generally result in higher PSD peaks (where coherence is typically high), but lower PSDs elsewhere, compared to the mean coherence approaches. The effect of user-defined aerodynamic regions compared to moving-segment analysis is more complicated and will be discussed for each of these four stations separately.

The station 8 PSD plot (Fig 21a) indicates that the MCM approach (red line) has much higher BFF rms levels, produced by a higher coherence than the baseline approach (blue line). This is shown by the broadband shift upwards in the MCM approach. This shift upwards is caused by removal of the artificial user-defined boundary, also seen in Figs. 19 and 20. The FCU approach (green) generally follows the baseline approach, with some minor changes in low and high frequencies. The FCM approach (black) provides a blend of the previous two approaches, incorporating the higher levels associated with the MCM approach at lower frequencies and the lower levels associated with the FCU approach at higher frequencies. This trend was one of the key observations from the BVT investigation in section IV.A.2 – mean coherence underpredicts higher amplitude BFF rms frequencies and overpredicts lower amplitude BFF rms frequencies.

BFFs developed for Station 16, the first transducer station downstream of an expansion corner, display different behavior than station 8. Figure 21b shows that the baseline approach (MCU) has the highest BFF rms levels at this condition, regardless of Mach number. The PSD of BFFs developed using moving-segment analysis are generally lower than their user-defined region counterparts. The lower values at this station can be attributed to the choice of aerodynamic region for the MCU- and FCU-developed BFFs. As discussed in Section IV.B.3, the moving-segment approach tends to gradually increase the local coherence lengths when compared to the user-defined aerodynamic regions. This trend can be observed in Figs. 17 and 18. A closer examination of the frequency-dependent coherence factors, Figs. 19 and 20, provides a second reason why the user-defined regions result in higher PSDs. The user-defined region that includes station 16 spans a large region of the vehicle starting with station 16 and ending at station 24, near the SRB forward attachment hardware. The coherence factors for this region are based on all the sensors within this region and assume the coherence length is constant across it (whether for the entire spectrum, or for each individual frequency). The moving-segment coherence factors are developed using just three transducer stations, and therefore represent a more localized flow field. The impact of this difference is more readily seen in Fig. 20. The coherence factors developed using the FCM approach are generally lower than those developed using the FCU approach in this region. One area where the coherence factors are higher is at low frequencies near the SRB nose cones. This region of high coherence factors is also present in the FCM method, but albeit with lower values. Ahead of this region, FCM shows low values for coherence factors, while the FCU approach results in higher values, especially at station 16. This increase is due to the coherence factors being based on both the more coherent flow near the SRBs and the less coherent flow further forward in this aerodynamic region. Using a large aerodynamic region, such as this one, results in a coherence length that is longer than needed in areas of low coherence and shorter than required in areas of high coherence, akin to the averaging used in MCU and MCM approaches.

The flow field around transducer station 26 is generally dominated by the interaction of shocks located on either side of the SRBs and the wake created by the SRB forward attachment hardware. This flow feature is associated with some of the highest buffet-related loads on the vehicle. This phenomenon manifests itself in the PSD plots (Fig. 21c) as a large, dominant peak and its harmonics. For $M = 0.90$, four peaks associated with this phenomenon can be discerned and at $M = 1.10$, three peaks are visible. At this station, all four methods for developing coherence factors result in PSDs where these dominant peaks are similar, i.e., have a coherence factor value of approximately 1. Away from the peaks, the frequency-dependent coherence factor approaches (FCU and FCM) result in lower PSD values. Furthermore, the moving-segment analysis also reduced the PSD values away from the peaks. This trend is explained in Figs. 17a and 18a, which compare the mean coherence lengths calculated using MCU and MCM approaches. The MCM approach indicates that the coherence lengths are relatively short for stations 25-27 and then begin to increase, reaching a maximum value for stations 31-33. The MCU approach employs a user-defined region that spans both these lower and higher coherence length regions, with a resulting coherence length falling in between the minimum and maximum values calculated by the MCM approach. This increases the coherence factors on the forward half of this segment, and artificially reduces them on the aft half of the segment, akin to the trend noted at station 16.

The final station examined is station 33, whose PSDs are presented in Fig. 21d. Many of the trends in the PSDs noted in the previously discussed stations are applicable to this station. One exception is the impact of moving-segment analysis compared to the user-defined aerodynamic region approach. The moving-segment analysis resulted in generally lower PSDs, compared to the user-defined region analysis (compare MCM versus MCU curves and FCM versus FCU curves in Fig. 21d.) The explanation for this opposite trend to the one noted for station 26 can be gleaned from Figs. 17a and 18a, which compare the mean coherence lengths calculated using MCU and MCM approaches. Station 33 is on the

boundary between region 6 (downstream of the SRB forward attachment) and region 7 (aft end of the vehicle). The moving-segment approach indicates that station 33 should be grouped with the sensors in region 6, which exhibit long coherence lengths, not with the aft section of the vehicle, which has relatively short coherence lengths. Making this adjustment in the boundary between these two regions resulted in much closer comparisons between the moving-segment approach-derived BFFs and the user-defined region-derived BFFs (not presented).

V. Conclusions

The accepted method for modeling the unsteady loads acting on a launch vehicle due to the transonic buffet environment requires wind tunnel testing of subscale rigid models instrumented with hundreds of miniature pressure transducers. Fluctuating surface pressures are acquired in a time correlated manner and subsequently are integrated over the surface of the vehicle to develop centerline orthogonal loads, commonly called buffet forcing functions (BFFs). The discrete nature of the pressure measurements requires that a series of adjustments are made to the integrated loads to account for the spatiotemporal variations in the pressures across the integration area associated with each sensor. The current approach used by the Space Launch System (SLS) project to calculate these adjustments, called coherence factors, divides the vehicle into a series of aerodynamic regions within which coherence lengths are assumed to be constant, and determines these coherence lengths based on a mean value of the coherence function over a specified frequency range.

The present work introduced two modifications to the development methodology of coherence factors. The first modification is to employ frequency-dependent coherence factors instead of coherence factors based on a mean of the coherence function, since coherence varies as a function of frequency. The other change replaces the aerodynamic regions with a moving-segment analysis that varies the calculated coherence lengths as a function of longitudinal location of the transducers. This approach calculates coherence length for overlapping segments of the vehicle that have a set number of transducer stations. At each station, the local coherence length is selected based on maximum value for the segments overlapping at that station.

The impact of these approaches was examined on (1) a notional launch vehicle geometry by comparing discrete measurement-based BFFs to those developed by continuous integration of unsteady pressure sensitive paint data and (2) the SLS Block 1 Crew vehicle by comparing the updated approaches to the program-accepted BFFs. To compare the user-defined region definition to the new moving-segment approach, the coherence lengths were determined using the mean coherence for a set frequency range for both approaches in order to isolate the effects of each. In general, the moving-segment approach resulted in similar coherence lengths, and therefore, similar coherence factors when compared to BFFs developed using the user-defined aerodynamic region approach. Comparing coherence lengths in long longitudinal aerodynamic regions, the coherence lengths near the forward end of these regions change more gradually when developed using the moving-segment analysis compared to the abrupt change produced by the user-defined region approach. Towards the aft ends of these aerodynamic regions, the moving-segment approach calculates longer coherence lengths than the user-defined aerodynamic region approach. From this observation, it can be surmised that the constant coherence length determined using the user-defined aerodynamic region approach is analogous to an average coherence length for the region. Utilizing frequency-dependent coherence factors resulted in reductions in BFF power spectral density functions at frequencies where coherence was low and increases, or no changes if mean-coherence factors were equal to one, at frequencies where coherence is high.

Ultimately, the updated coherence factor approaches are both conceptually more intuitive and produce more intuitive results when compared to the current program-accepted approach, and are a more reliable estimation of the buffet environment via the discrete pressure transducer methods. Future work includes using uPSP data to glean further insight into the unsteady transonic pressure environment. While still in the early stages of development, uPSP research has nevertheless provided encouraging results [13–15]. But until uPSP is fully vetted, BFF development will rely on discrete pressure transducer methodology, and using frequency-based coherence and moving-segment aerodynamic regions are a recommended update to coherence methodology.

References

[1] Cole, H. A., Jr., Erickson, A. L., and Rainey, A. G., "Buffeting during atmospheric ascent," NASA SP-8001, Nov. 1970.

[2] Ericsson, L. E., "Unsteady Flow Separation Can Endanger the Structural Integrity of Aerospace Launch Vehicles," *Journal of Spacecraft and Rockets*, Vol. 38, 2001, pp. 168–179. https://doi.org/10.2514/2.3690.

[3] Robinson, R. C., Wilcox, P. R., Gambucci, B. J., and George, R. E., "Dynamic Response of a Family of Axisymmetric Hammerhead Models to Unsteady Aerodynamic Loading," Tech. rep., NASA TN D-4504, 1968.

[4] Sekula, M. K., Piatak, D. J., and Rausch, R. D., "Space Launch System Program (SLSP) Vehicle Aerodynamic Substantion Report for the SLS-1000X Buffet Forcing Function Database," NASA TM-2018-21930, May 2018.

[5] Piatak, D. J., Sekula, M. K., Rausch, R., Florance, J. R., and Ivanco, T. G., "Overview of the Space Launch System Transonic Buffet Environment Test Program," *53rd AIAA Aerospace Sciences Meeting, AIAA SciTech Forum*, 2015. https://doi.org/10.2514/6.2015-0557.

[6] Schuster, D. M., Panda, J., Ross, J. C., Roozeboom, N. H., Burnside, N. J., Ngo, C. L., Kumagai, H., Sellers, M., Powell, J. M., Sekula, M. K., and Piatak, D. J., "Investigation of Unsteady Pressure-Sensitive Paint (uPSP) and a Dynamic Loads Balance to Predict Launch Vehicle Buffet Environments," NASA TP-2016-219352, Nov. 2016.

[7] Sekula, M. K., Piatak, D. J., Rausch, R. D., Ross, J. C., and Sellers, M. E., "Assessment of Buffet Forcing Function Development Process Using Unsteady Pressure Sensitive Paint," *AIAA Aviation 2019 Forum*, American Institute of Aeronautics and Astronautics, 2019. https://doi.org/10.2514/6.2019-3503.

[8] Panda, J., "Verification of Calculation Procedure for Unsteady Aerodynamic Forces on a Launch Vehicle," *Journal of Spacecraft and Rockets*, Vol. 56, No. 6, 2019, pp. 1714–1724. https://doi.org/10.2514/1.a34490.

[9] Sekula, M. K., Piatak, D. J., and Rausch, R., "Effect of Surface Pressure Integration Methodology on Launch Vehicle Buffet Forcing Functions," *54th AIAA Aerospace Sciences Meeting*, 2016. https://doi.org/10.2514/6.2016-0545, URL https://arc.aiaa.org/doi/abs/10.2514/6.2016-0545.

[10] Sekula, M. K., Piatak, D. J., Rausch, R., Florance, J. R., and Ramey, J., "Initial Assessment of Space Launch System Transonic Unsteady Pressure Environment," *53rd AIAA Aerospace Sciences Meeting, AIAA SciTech Forum*, 2015. https://doi.org/10.2514/6.2015-0558.

[11] Brauckmann, G. J., Streett, C. L., Kleb, W. L., Alter, S. J., Murphy, K. J., and Glass, C. E., "Computational and Experimental Unsteady Pressuresfor Alternate SLS Booster Nose Shapes," *53rd AIAA Aerospace Sciences Meeting, AIAA SciTech Forum*, 2015. https://doi.org/10.2514/6.2015-0559.

[12] Alter, S. J., Brauckmann, G. J., Kleb, B., Glass, C. E., Streett, C. L., and Schuster, D. M., "Time-Accurate Unsteady Pressure Loads Simulated forthe Space Launch System at Wind Tunnel Conditions," *33rd AIAA Applied Aerodynamics Conference, AIAA AVIATION Forum*, 2015. https://doi.org/10.2514/6.2015-0557.

[13] Roozeboom, N., Baerny, J. K., Murakami, D. D., Ngo, C., and Powell, J. M., "Recent Developments in NASA's Unsteady Pressure-Sensitive Paint Capability," *AIAA Scitech 2020 Forum*, 2020. https://doi.org/10.2514/6.2020-0516.

[14] Soranna, F., Heaney, P. S., Sekula, M. K., Piatak, D. J., Ramey, J. M., Roozeboom, N., Murakami, D. D., Baerny, J. K., Li, J., Stremel, P. M., and Powell, J. M., "Analysis of Buffet Forcing Functions Estimated from Unsteady Pressure Sensitive Paint," *AIAA AVIATION 2020 FORUM*, 2020. https://doi.org/10.2514/6.2020-2685.

[15] Heaney, P. S., Soranna, F., Sekula, M. K., Piatak, D. J., and Ramey, J. M., "Analysis of Transonic Unsteady Aerodynamic Environments using Unsteady Pressure Sensitive Paint for the Space Launch System Block 1 Cargo Launch Vehicle," *AIAA SciTech 2021 Forum*, 2021.